Appl Phys B (2012) 106:613–618
DOI 10.1007/s00340-011-4750-6

Applied Physics B
Lasers and Optics

Hyperfine structure and absolute frequency measurements of $^{127}I_2$ transitions with monolithic Nd:YAG 561-nm lasers

T. Yang · F. Meng · Y. Zhao · Y. Peng · Y. Li · J. Cao · C. Gao · Z. Fang · E. Zang

Received: 27 May 2011 / Revised version: 16 August 2011 / Published online: 11 October 2011

Abstract The precision hyperfine structures of the $^{127}I_2$ transitions at 561.4 nm are measured by the heterodyne beat between two home-made $^{127}I_2$-stabilized Nd:YAG lasers. The theoretical distributions of the observed transitions' hyperfine sublevels are used to identify the two transitions. High-accuracy hyperfine constants are obtained by fitting the measured hyperfine splittings to the four-term Hamiltonian, which includes the electric quadruple, spin-rotation, tensor spin–spin and scalar spin–spin interactions. The absolute frequencies of the observed four transitions are measured by an optical frequency comb based on a mode-locked erbium-fiber laser.

1 Introduction

The monolithic nonplanar ring Nd:YAG laser has been proved to show many advantages, such as stable single-frequency operation, very low resonator loss, excellent open-loop frequency and power stability, wide continuous tuning range, narrow-linewidth and high output power [1, 2]. As a suitable and stable coherent laser source, the monolithic laser has been used widely in laser frequency stabilization and hyperfine spectroscopy. The 532-nm $^{127}I_2$-stabilized Nd:YAG lasers have been recommended for the realization of the SI base unit "meter" by the International Committee for Weights and Measures (Comité International des Poids et Mesures—CIPM/BIPM) [3]. The Doppler-broadened absorption transitions of molecular iodine from 500 nm to 675 nm had been measured by S. Gerstenkorn and P. Luc in 1979 [4]. The hyperfine structure and hyperfine constants of the $^{127}I_2$ transitions has been tabulated by A. Razet and S. Picard [5]. The calculation method of the hyperfine structures and hyperfine constants of the $^{127}I_2$ $B^3\Pi^+_{0_u}$–$X^1\Sigma^+_g$ transitions was described by S. Picard and A. Razet [6, 7]. In the past three decades, hyperfine structures of $^{127}I_2$ transitions in many wavelength regions have been studied, such as 515 nm [8–10], 532 nm [11–13], 560 nm [14], 578 nm [15], 633 nm [16–18] etc. However, the high-precision spectroscopy of the $^{127}I_2$ transitions essentially depends on the availability of suitable laser sources.

In the present paper, we report two home-made Nd:YAG nonplanar monolithic 1123-/561-nm lasers which are locked to the hyperfine components of the four observed transitions of $^{127}I_2$ at 561.4 nm via the modulation transfer spectroscopy (MTS) [19, 20]. The high-precision measurement of the hyperfine structure components of the four $^{127}I_2$ transitions at 561.4 nm are obtained by the heterodyne beat of two $^{127}I_2$-stabilized Nd:YAG lasers. Fitted hyperfine constants of the transitions are computed. The absolute frequencies of the observed transitions are measured with an optical frequency comb (OFC). Since the absorption strength of the observed $^{127}I_2$ P(58)22-1 and R(62)22-1 transitions is similar to the $^{127}I_2$ R(56)32-0:a_{10} transition near 532 nm,

T. Yang (✉) · C. Gao
School of Opto-Electronics, Beijing Institute of Technology, 25 South Zhongguancun Street, Haidian District, Beijing 100081, P.R. China
e-mail: tyang@bit.edu.cn
Fax: +86-10-64524558

T. Yang · F. Meng · Y. Li · J. Cao · Z. Fang · E. Zang
Center of Time and Frequency Metrology, National Institute of Metrology, 18 Beisanhuan East Rd, Chaoyang District, Beijing 100013, P.R. China

E. Zang
e-mail: ejzang@nim.ac.cn

Y. Zhao · Y. Peng
Department of Precision Instruments and Mechanology, Tsinghua University, Beijing 100084, P.R. China

the observed transitions are considered to be important frequency references in the 561-nm region. A 561-nm optical frequency standard can be used in multi-wavelength interferometry for gauge block measurements. The coherent radiation of a frequency-stabilized 1123-nm wavelength also has potential applications in areas of differential absorption lidar to allow remote monitoring of atmospheric water vapor concentration.

2 Experiment setup

Figure 1 shows the optical schematic illustration of the $^{127}I_2$-stabilized laser via the MTS. The home-made Nd:YAG 1123-nm single-frequency 1-W laser has been developed by using the monolithic nonplanar ring oscillator [19]. In a single pass through the PPMgO:LN second-harmonic generation crystal, the 561-nm output power is typically about 10 mW with more than 500-mW incident power at 1123 nm at 30°C. Two independent 45-cm length iodine cells are used for each of the two lasers and the cooling finger temperatures of the two cells are both set to −18°C, corresponding to a vapor pressure of 0.54 Pa. A 4-pass $^{127}I_2$-absorption cell configuration is adopted in the optical setup. Two right angle prisms located at the two ends of the cell, as shown in Fig. 1, are used to fold the optical beam twice in both the horizontal and vertical planes. This multi-pass scheme makes the optical beam passing through the iodine cell four times, and the total absorption length is 1.8 m. The beam diameter of the first laser is 2.5 mm and the second is 4 mm. A combination of a λ/2 plate and a polarization beamsplitter (PBS) is used to generate a proper power ratio for the pump and probe beams. In the first system, the pump power is set to 1.0 mW and the probe power is 0.2 mW. The second laser uses 4.1-mW pump power and 1.0-mW probe power. The pump and probe beams are overlapped and accurately counter-propagate within the iodine cell. The pump beams of the two lasers are frequency-shifted 80 MHz by acousto-optic modulators (AOM) and phase-modulated by electro-optic modulators (EOM). The driving signal of the AOM comes from a synthesizer referenced to a rubidium clock. The −1 and +1 order diffraction of the AOM is taken in the first and second $^{127}I_2$-stabilized lasers, respectively, which avoids zero frequency beat between the two lasers. The EOM modulation frequency is 277 kHz in the first system and 250 kHz in the second. The unmodulated probe beam passes through the iodine cell, and is steered by a PBS onto a photodiode. A beamsplitter is used to separate the first laser 1123-nm output into two beams as shown in Fig. 2. One is used to detect the hyperfine splittings of the observed transitions, and the other beam is used to measure the absolute frequency of the observed transition by an OFC. The first laser is locked to one component of the observed

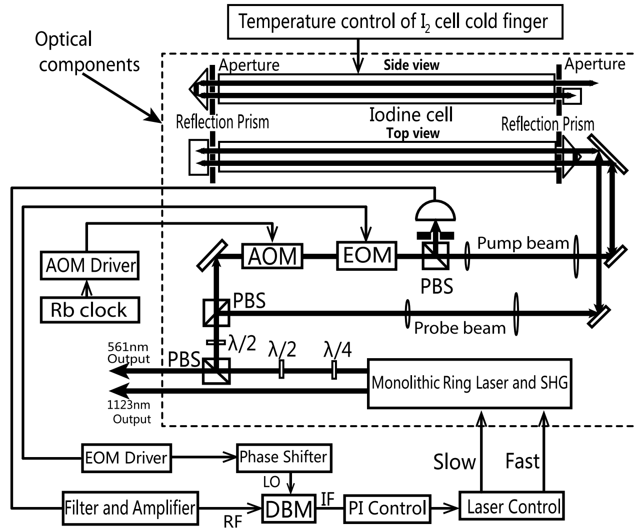

Fig. 1 Schematic illustration of the experiment. PBS, polarization beam splitter; λ/2, half-wave plate; λ/4, quarter-wave plate; AOM, acousto-optic modulator; EOM, electro-optic modulator; PD, photodiode; DBM, double-balance mixer

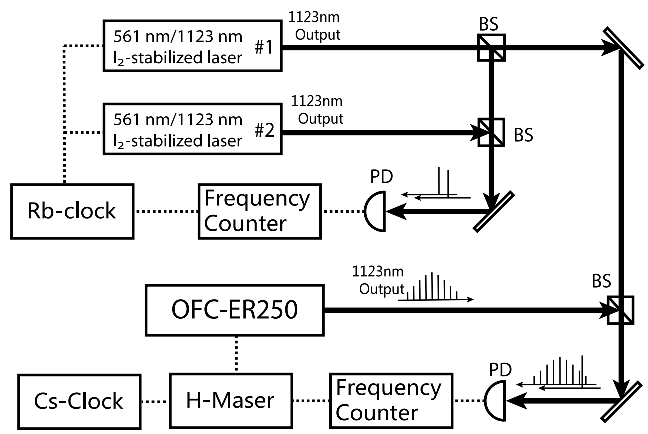

Fig. 2 Schematic illustration of the experiment. BS, beam splitter; PD, photodiode; OFC-Er250, an optical frequency comb based on a mode-locked Er-droped-fiber laser

$^{127}I_2$ transitions. The second laser is locked to each of the other components of the observed transitions, respectively. At the same time, the heterodyne beat-note signal between an OFC and the first laser at 1123 nm is measured by using a photodiode followed by a frequency counter, as shown in Fig. 2. The frequency counter and the OFC are referenced to an H-maser, which is calibrated by the Cs fountain clock in our institute.

3 Measurements and results

Thirty hyperfine structure components of the $^{127}I_2$ transitions at 561.437 nm are observed as shown in Fig. 3, which

Table 1 Observed and calculated hyperfine splittings of the $^{127}I_2$ R(62)22-1 and P(58)22-1 transition

Measurement sequence	Observed (MHz)	R(62)22-1			P(58)22-1		
		Hyperfine component	Calculated (MHz)	Obs. − Cal. (MHz)	Hyperfine component	Calculated (MHz)	Obs. − Cal. (MHz)
1	0.000	a_1	0.000	0.000			
2	110.240				a'_1	110.240	0.000
3	270.589	a_2	270.884	0.295			
4	286.669	a_3	286.616	−0.053			
5	290.258	a_4	290.249	−0.009			
6	305.957	a_5	306.085	0.127			
7	381.707				a'_2	381.931	0.223
8	396.319				a'_3	396.304	−0.015
9	401.088				a'_4	401.073	−0.015
10	412.303	a_6	412.444	0.141			
11	415.296				a'_5	415.528	0.232
12	424.950	a_7	424.989	0.039			
13	439.685	a_8	439.634	−0.052			
14	452.077	a_9	452.591	0.514			
15	522.787				a'_6	522.887	0.101
16	535.680				a'_7	535.699	0.019
17	549.352				a'_8	549.367	0.015
18	562.547				a'_9	562.639	0.092
19	576.758	a_{10}	576.663	−0.095			
20	686.974				a'_{10}	686.91	−0.064
21	708.842	a_{11}	708.837	−0.006			
22	711.784	a_{12}	711.707	−0.077			
23	730.070	a_{13}	729.941	−0.129			
24	734.126	a_{14}	734.033	−0.093			
25	819.324				a'_{11}	819.315	−0.009
26	821.939				a'_{12}	821.879	−0.060
27	840.336				a'_{13}	840.267	−0.069
28	844.167				a'_{14}	844.157	−0.010
29	865.569	a_{15}	865.442	−0.127			
30	975.812				a'_{15}	975.724	−0.089

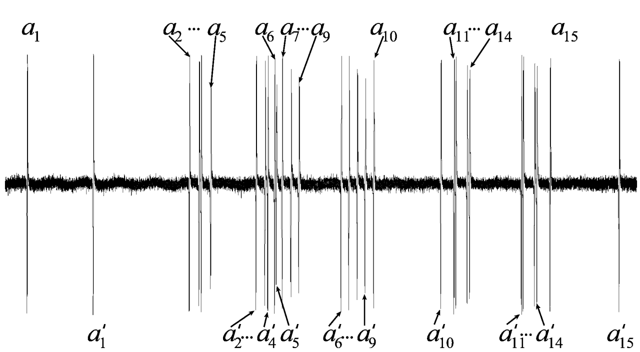

Fig. 3 Modulation transfer spectroscopy signal of the $^{127}I_2$ P(58)22-1 and R(62)22-1 transition

belong to the $^{127}I_2$ P(58)22-1 transition and the R(62)22-1 transition, respectively. These two transitions have the same absorption strength and are very close to each other. It is very difficult to identify these two transitions. The frequency differences between the first component from the red end of the observed transition band and each of the other hyperfine components are measured and shown in Table 1. These observed transitions are measured preliminarily by a wavemeter (WA1500 from EXFO Co.). The R(130)24-1 transition is observed at 561.431 nm and the R(103)23-1 transition is at 561.427 nm. Figure 4 shows the MTS signals of the $^{127}I_2$ R(130)24-1 and R(103)23-1 transitions. The signal to noise ratio of the R(103)23-1 transition is 13 dB in a 1-kHz bandwidth, which is stronger than the R(130)24-1 transition

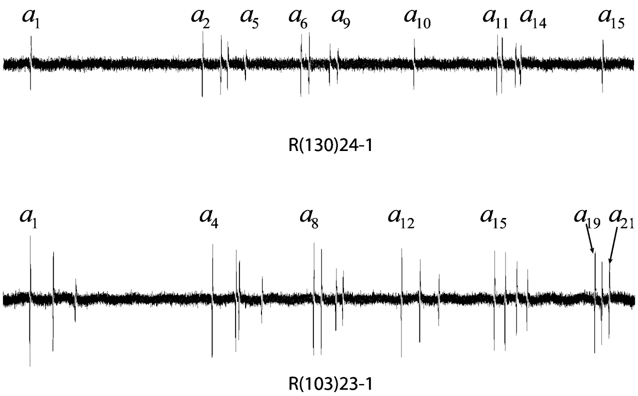

Fig. 4 Modulation transfer spectroscopy signal of the $^{127}I_2$ R(130)24-1 and R(103)23-1 transition

(7 dB in a 1-kHz bandwidth), and weaker than the P(58)22-1 and R(62)22-1 transitions. The signal to noise ratio of the P(58)22-1 and R(62)22-1 transitions is about 17 dB in a 1-kHz bandwidth. The linewidth of the 15th component of the P(58)22-1 transitions is about 950 kHz. The hyperfine splittings of the R(103)23-1 and R(130)24-1 transitions are shown in Tables 2 and 3, respectively. Each measured frequency value in the Tables 1–3 is an averaging of 1000 beat frequency measurements, where each beat frequency is measured with 1-s gate time by a frequency counter. The standard deviation of the 1000 beat frequency data is typically less than 260 Hz for the two transitions at 561.4367 nm, 650 Hz for the R(103)23-1 transition and 2.3 kHz for the R(130)24-1 transition, respectively.

According to the $^{127}I_2$ transition theory, the high frequency stability and high-accuracy measurements will reduce the theoretical deviation of hyperfine frequency distributions and increase the accuracy of the hyperfine constants [7]. Based on the optimized theoretical distributions of the $^{127}I_2$ 30 hyperfine sublevels, the hyperfine components $a_1 - a_{15}$ belongs to the R(62)22-1 transition, and $a'_1 - a'_{15}$ are the P(58)22-1 transition as shown in Table 1. The agreements between calculations and measurements are less than 0.5 MHz. The distributions of the observed 21 or 15 hyperfine sublevels are compared with the calculation results as shown in Tables 2 and 3, the frequency difference between the calculations of the R(103)23-1 and R(103)24-1 transitions and measurements are less than 0.35 MHz. The hyperfine constants for the observed transitions using the four-term Hamiltonian is determined by the measured $^{127}I_2$ hyperfine spectra [21]. The Hamiltonian of the hyperfine interaction, H_{hfs}, can be written as

$$H_{fhs} = eQq \times H_{EQ} + C \times H_{SR} + d \times H_{TSS} + \delta \times H_{SSS}, \quad (1)$$

where H_{EQ}, H_{SR}, H_{TSS}, and H_{SSS} represent, respectively, the electric quadruple, spin–rotation, tensor spin–spin, and scalar spin–spin interactions and eQq, C, d, and δ represent the corresponding hyperfine constants for each of these

Table 2 Observed and calculated hyperfine splittings of the R(103)23-1 transition

Hyperfine component	Observed (MHz)	Calculated (MHz)	Obs. − Cal. (MHz)
a_1	0.000	0.000	0.000
a_2	34.780	35.125	−0.345
a_3	69.481	69.337	0.144
a_4	283.734	283.752	−0.018
a_5	320.600	320.818	−0.218
a_6	325.705	325.900	−0.195
a_7	362.089	361.996	0.093
a_8	443.499	443.550	−0.051
a_9	455.509	455.626	−0.117
a_{10}	478.932	478.999	−0.067
a_{11}	489.735	489.702	0.033
a_{12}	582.423	582.412	0.011
a_{13}	611.453	611.553	−0.100
a_{14}	641.551	641.307	0.244
a_{15}	729.133	729.142	−0.009
a_{16}	746.185	746.214	−0.029
a_{17}	764.547	764.549	−0.002
a_{18}	781.267	781.222	0.045
a_{19}	888.425	888.394	0.031
a_{20}	899.149	899.137	0.012
a_{21}	911.043	910.986	0.057

Table 3 Observed and calculated hyperfine splittings of the R(130)24-1 transition

Hyperfine component	Observed (MHz)	Calculated (MHz)	Obs.−Cal. (MHz)
a_1	0.000	0.000	0.000
a_2	255.273	255.531	−0.258
a_3	282.793	282.773	0.020
a_4	293.135	293.114	0.021
a_5	320.372	320.630	−0.258
a_6	404.095	404.202	−0.107
a_7	416.258	416.275	−0.017
a_8	447.392	447.405	−0.013
a_9	459.478	459.582	−0.104
a_{10}	575.914	575.839	0.075
a_{11}	702.029	702.022	0.007
a_{12}	709.480	709.407	0.073
a_{13}	730.264	730.184	0.080
a_{14}	738.201	738.203	−0.002
a_{15}	864.150	864.053	0.097

Table 4 The fitted hyperfine constants of the observed transitions

	R(62)22-1	P(58)22-1	R(103)23-1	R(130)24-1
ΔeQq (MHz)	1923.91(22)	1924.08(12)	1923.30(14)	1920.42(14)
ΔC (kHz)	47.86(48)	48.07(30)	52.43(10)	56.93(14)
$\Delta\delta$ (kHz)	4.16(0)	4.16(0)	3.64(0)	3.10(0)
Δd (kHz)	14.74(26)	14.74(14)	14.92(16)	15.12(16)

interactions [22]. By theoretically fitting the observed spectra of the transitions, accurate values of the observed transitions' hyperfine constants ΔeQq, ΔC, $\Delta\delta$, and Δd are obtained, as shown in Table 4.

The absolute frequencies of the observed $^{127}I_2$ transitions are measured by an OFC based on a mode-locked erbium-fiber laser [23, 24]. The repetition rate of the frequency comb (f_{rep}) is about 250 019 820 Hz, and the offset frequency (f_{ceo}) is set to 20 MHz. The frequency shift of the laser induced by AOM (f_{AOM}) is 20 MHz. When the 1123-nm output laser beam of the first $^{127}I_2$-stabilized laser beats with the nth comb mode at the frequency of f_{beat}, the absolute frequency of the measured Nd:YAG laser can be calculated as

$$f = nf_{rep} + f_{ceo} - f_{AOM} \pm f_{beat}, \quad (2)$$

where the f_{rep} and f_{ceo} are locked to the H-maser. The uncertainty of the H-maser is 1.2×10^{-12} for a 1-s averaging time. The averaged frequency of the $^{127}I_2$ P(58)22-1:a'_{15} transition is about 533 974 000 250 kHz. The standard deviation of the measurements is 4.0 kHz. The averaged frequency of the R(103)23-1:a_1 hyperfine component is about 533 983 045 975 ± 6 kHz, and the averaged frequency of the R(130)24-1:a_1 is about 533 978 765 860 ± 12 kHz. The repeatability of the three measurements are checked during 10 different days as shown in Figs. 5–7. The repeatability of the measurements is limited to the repeatability of the $^{127}I_2$-stabilized laser.

4 Conclusion

In this paper, two Nd:YAG nonplanar monolithic 1123-/561-nm lasers are developed to observe the modulation transfer spectroscopy signal of the four $^{127}I_2$ ro-vibrational transitions at 561.4 nm. The high-precision measurement of the hyperfine structure components of these four transitions are obtained by the heterodyne beat between the two lasers. The theoretical hyperfine structure frequency distributions of the observed transitions are calculated, and hyperfine constants of $^{127}I_2$ transitions at 561.4 nm are fitted according to the $^{127}I_2$ $B^3\Pi^+_{0_u} - X^1\Sigma^+_g$ theory. The calculations match very well with the measurement results. The absolute frequencies of the observed transitions are measured with an

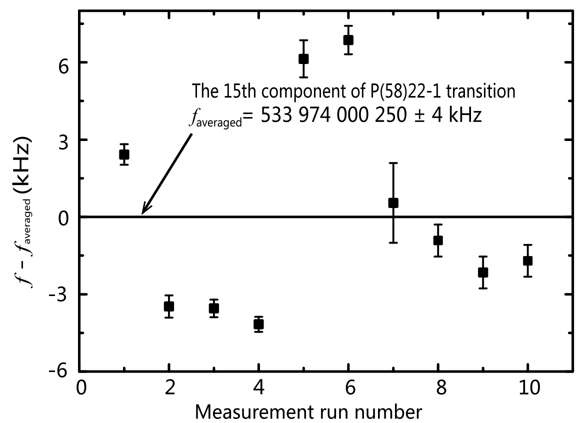

Fig. 5 The absolute frequency of the 15th component of the P(58)22-1 transition

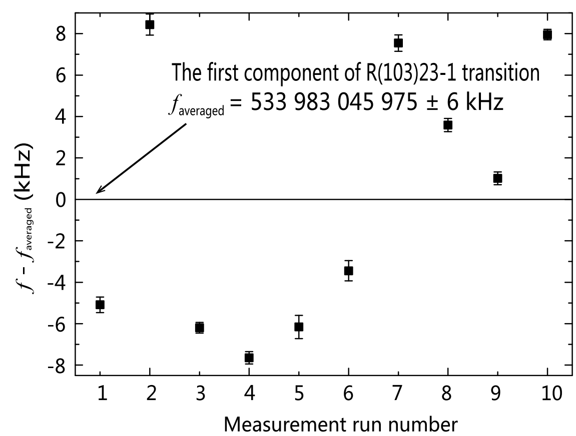

Fig. 6 The absolute frequency of the first component of the R(130)24-1 transition

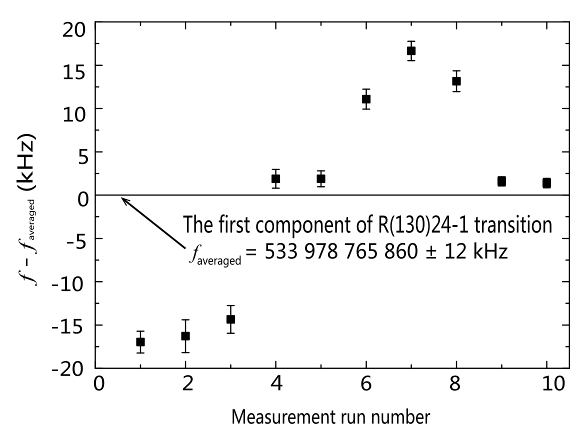

Fig. 7 The absolute frequency of the first component of the R(103)23-1 transition

optical frequency comb. The high-precision measurements and calculations are helpful to improve the $^{127}I_2$ transition hyperfine database, and the calculation precision of the $^{127}I_2$ hyperfine structure at 561 nm. The observed transitions are considered to be important frequency references in the 561-nm region.

Acknowledgements We acknowledge many valuable discussions with Dr. F.-L. Hong in National Metrology Institute of Japan, Dr. L.-S. Chen in Wuhan Institute of Physics and Mathematics, Chinese Academy of Science and Dr. X.-Z. Chen in Peking University. This work is supported by the National Nature Science Foundation of China (grants 60727005, 60178009 and 60478032) and National major research program, China (2010CB922902).

References

1. T.J. Kane, R.L. Byer, Opt. Lett. **10**, 65 (1985)
2. E.A.P. Cheng, T.J. Kane, Opt. Lett. **16**, 478 (1991)
3. T.J. Quinn, Metrologia **40**, 103 (2003)
4. S. Gerstenkor, P. Luc, *Atlas du Spectre d'Absorption de la Molecule d'Iode* (Edition du CNRS, Paris, 1978)
5. A. Razet, S. Picard, Metrologia **33**, 19 (1996)
6. S. Picard, Rapport BIPM-90/5 (1990)
7. S. Picard, A. Razet, Rapport BIPM-91/2 (1991)
8. H.J. Foth, F. Spieweck, Chem. Phys. Lett. **65**, 347 (1979)
9. R.J. Jones, W.Y. Cheng, K.W. Holman, L. Chen, J.L. Hall, J. Ye, Appl. Phys. B, Lasers Opt. **74**, 597 (2002)
10. J.-P. Wallerand, L. Robertsson, L.-S. Ma, M. Zucco, Metrologia **43**, 294 (2006)
11. J.L. Hall, L.-S. Ma, M. Taubman, B. Tiemann, F.L. Hong, O. Pfister, J. Ye, IEEE Trans. Instrum. Meas. **48**, 583 (1999)
12. E.-J. Zang, J.-P. Cao, Y. Li, C.-Y. Li, Y.-K. Deng, C.-Q. Gao, IEEE Trans. Instrum. Meas. **56**, 673 (2007)
13. G. Galzerano, C. Svelto, E. Bava, F. Bertinetto, Appl. Opt. **38**, 6962 (1999)
14. J. Zhang, Z.H. Lu, L.J. Wang, Appl. Opt. **48**, 5629 (2009)
15. F.-L. Hong, H. Inaba, K. Hosaka, M. Yasuda, A. Onae, Opt. Express **17**, 1652 (2009)
16. J. Lazar, O. Číp, P. Jedlička, Appl. Opt. **39**, 3085 (2000)
17. H.R. Simonsen, F. Rose, Metrologia **37**, 651 (2000)
18. J. Hu, E. Ikonen, K. Riski, Metrologia **33**, 467 (1996)
19. E.-J. Zang, J.-P. Cao, Y. Li, T. Yang, D.M. Hong, Opt. Lett. **32**, 250 (2007)
20. T. Yang, J.-P. Cao, Y. Li, Z.-J. Fang, C.-Q. Gao, E.-J. Zang, in *Precision Electromagnetic Measurements (CPEM), 2010 Conference* (2010), pp. 115–116
21. F.-L. Hong, J. Ye, L.-S. Ma, S. Picard, C.J. Bordé, J.L. Hall, J. Opt. Soc. Am. B **18**, 379 (2001)
22. B. Bodermann, H. Knöckel, E. Tiemann, Eur. Phys. J. D **19**, 31 (2002)
23. J. Ye, J.-L. Peng, R.J. Jones, K.W. Holman, J.L. Hall, D.J. Jones, S.A. Diddams, J. Kitching, S. Bize, J.C. Bergquist, L.W. Hollberg, L. Robertsson, L.-S. Ma, J. Opt. Soc. Am. B **20**, 1459 (2003)
24. J.L. Peng, H. Ahn, R.H. Shu, H.C. Chui, J.W. Nicholson, Appl. Phys. B, Lasers Opt. **86**, 49 (2007)